Pak. J. Bot., 57(5): 1761-1768, 2025. DOI: http://dx.doi.org/10.30848/PJB2025-5(38)

REGULATORY NETWORKS AND METABOLITE VARIATIONS DURING LEAF GROWTH AND DEVELOPMENT IN *DRYNARIA ROOSII* NAKAIKE

HONGYU CHEN[1,2,3], BO WANG[1,2,3], YING YU[4] AND QINGWEN SUN[1,2,3*]

[1]*School of Pharmaceutical Sciences, Guizhou University of Traditional Chinese Medicine, Guiyang 550025, China*
[2]*Guizhou Key Laboratory for Raw Material of Traditional Chinese Medicine, Guiyang, China*
[3]*Research Center of Medical Fern Resources and Development, Guizhou University of Traditional Chinese Medicine, Guiyang, China*
[4]*School of Basic Medicine, Guizhou University of Traditional Chinese Medicine, Guiyang, China*
[*]*Corresponding author's email: sqw1978_2006@126.com*

Abstract

Leaf development is a pivotal stage in the plant life cycle, involving intricate physiological and morphogenetic processes characterized by dynamically shifting molecular mechanisms and metabolite patterns, which have not been extensively studied in the traditional medicinal plant *Drynaria roosii* Nakaike. This study utilized next-generation sequencing to profile the leaf transcriptome of *D. roosii*, identifying significant differences in gene expression between two distinct developmental stages, with a focus on transcription factors that regulate leaf formation and metabolite production. *De novo* assembly of high-quality sequences generated 82,476 unigenes of average length 1,292 bp. FPKM analysis unveiled substantial transcriptome changes during leaf development. Additionally, non-targeted metabolomics detected 1,297 compounds across both stages, with lipids representing the most abundant metabolite group. This study offers dynamic insights into transcriptomic and metabolomic shifts during *D. roosii* leaf development, elucidates crucial regulatory networks involved in this process, and enhances the annotation of the *D. roosii* genome, paving the way for future investigations.

Key words: *Drynaria roosii*; Leaf; Development; Regulatory networks; Metabolite accumulation.

Introduction

Leaf development represents a fundamental phase in the plant life cycle, characterized by a series of intricate and dynamic processes involving numerous genes that determine leaf morphology, size, photosynthetic capacity, and metabolite landscapes. Advanced next-generation sequencing (NGS) technologies (e.g., Roche/454 and Illumina High-Seq) have revolutionized genomic research by providing lower-cost high-throughput sequencing compared to traditional methods, leading to numerous studies employing *de novo* sequencing, genome resequencing, and transcriptome analysis (Gase, 2012). Such studies have yielded critical functional insights into the molecular mechanisms governing gene expression (Morozova & Marra, 2008), especially in non-model organisms without reference genomes like *Drynaria roosii* Nakaike (Sun *et al*., 2018). The extensive genomic and transcriptomic data generated by NGS support various applications, including gene discovery and localization, gene expression studies, comparative genomics, and molecular marker development. For example, transcriptomic studies using Illumina paired-end sequencing was researched in several plant species, such as *Apium graveolens* L. (Jia *et al*., 2015), *Bergera koenigii* L. (Shivakumar *et al*., 2019), *Eucommia ulmoides* (Li *et al*., 2019), *Panicum virgatum* L. (Palmer *et al*., 2019), *Osmanthus fragrans* (Chen *et al*., 2020), *Brassica campestris* L. (Shi *et al*., 2023), and *Epimedium pubescens* (Xu *et al*., 2023).

As a complementary approach to transcriptomics, metabolite profiling has been a powerful tool for exploring leaf developmental changes, revealing that metabolite levels significantly influence plant phenotypes. Data obtained from this approach have enhanced our understanding of dynamic metabolite changes occurring during leaf development (Zhang *et al*., 2018; Li *et al*., 2019; Xu *et al*., 2023) and enabled the identification of metabolism products and their functional roles within metabolic networks and pathways (Töpfer *et al*., 2015; Chang *et al*., 2024). Integrating metabolomics with transcriptomics has enhanced our understanding of biosynthetic mechanisms related to essential metabolic pathways (Li *et al*., 2018; Zhu *et al*., 2018), particularly those involved in the synthesis and retention of medicinally important bioactive compounds in plant tissues (Nett *et al*., 2020; Lau & Sattely, 2015).

Despite these advancements, the molecular and biochemical processes regulating leaf growth and development in the traditional Chinese medicinal plant *D. roosii*, known as GuSuiBu in China (Sun *et al*., 2017; Sun *et al*., 2018; Wufuer *et al*., 2020; Chang *et al*., 2024), remain poorly understood due partly to limited transcriptomic data across its developmental stages. In this study, we employed Illumina paired-end sequencing to construct a comprehensive transcriptome database for *D. roosii* leaves at two distinct developmental stages while concurrently conducting metabolome profiling to categorize leaf metabolites and examine dynamic changes in their accumulation. All of the discoveries of this study may dig new acknowledgement on the interacted mechanisms underlying metabolite biosynthesis and regulation during *D. roosii* leaf growth and development, highlighting the importance of certain integrated approaches in elucidating these processes.

Material and Methods

Plant materials: *D. roosii* plants were obtained from the medicinal plant resource nursery of Guizhou University of Traditional Chinese Medicine in March 2024. For transcriptome analysis, two growth stages were selected, designated as Stage1 and Stage2, with representative tissues collected for every stage (Fig. 1). Four experimental replicates were setted for every stage, using ten leaves from a single plant per replicate. Each sample was examined using three biological replicates. For metabolome analysis, six experimental replicates were analyzed for every growth stage.

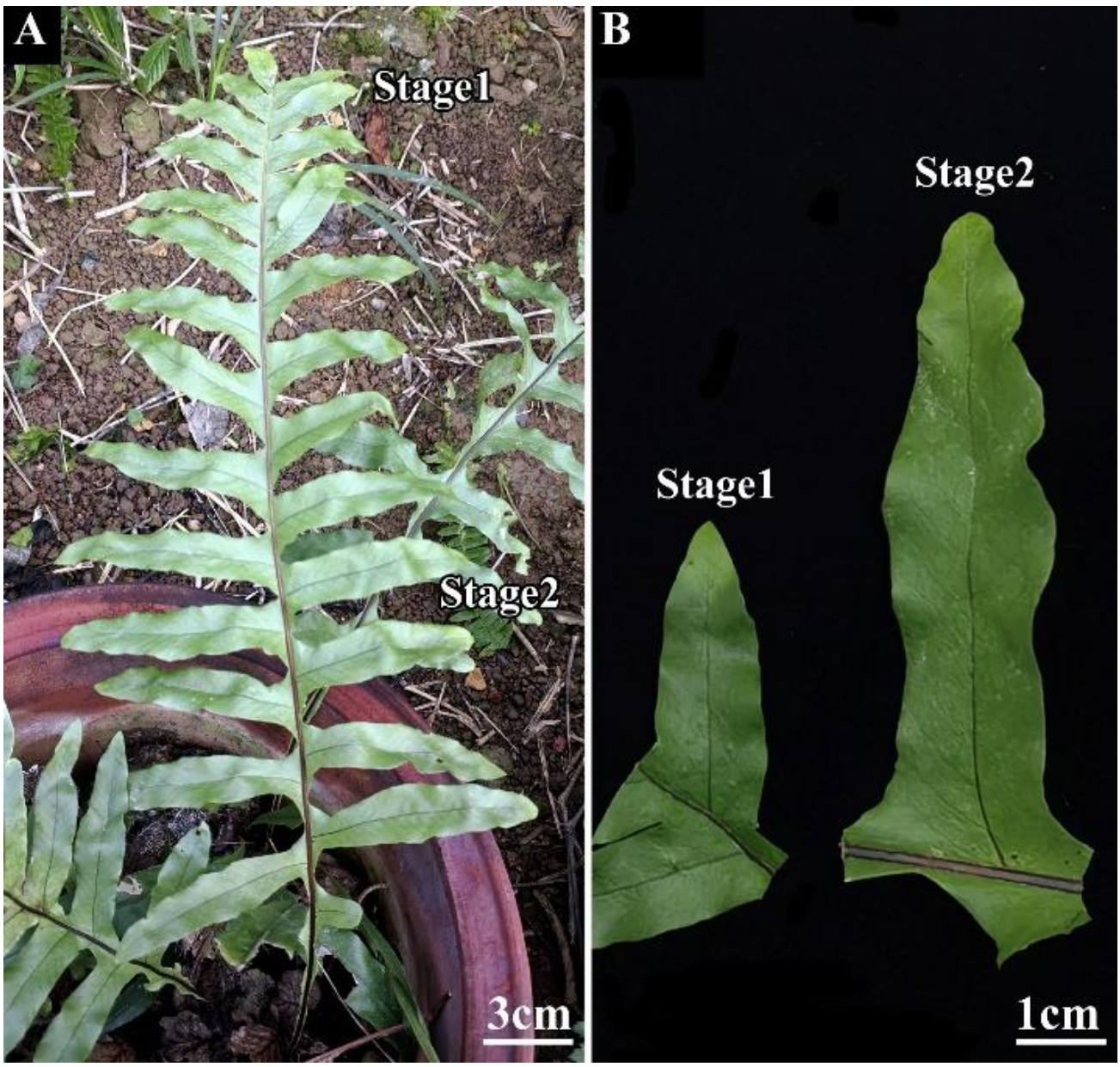

Fig. 1. Morphological characterization of *D. roosii* leaves at different growth stages.

RNA preparation and Illumine analysis: We isolated the total RNA extracts from leaves through the cetyltrimethylammonium bromide (CTAB) method, followed by assessments of RNA's purity, RNA integrity number (RIN), 28S/18S ratio, and fragment length distribution, which were performed through Agilent 2100 Bioanalyzer (RNA 6000 Nano Kit, Takara, Beijing, China). Additionally, a NanoDrop spectrophotometer was used to assess RNA purity then the RNA samples were sent to the Beijing Genomics Institute (BGI) for further purification followed by library construction and RNA-Seq.

To obtain clean reads, SOAPnuke (v1.6.5) was introduced to filter raw sequencing data, and the treated data was then saved in FASTQ format (Chen *et al*., 2018). Trinity (v2.13.2) was adopted to assemble the clean reads into contigs, Benchmarking Universal Single-Copy Orthologs (BUSCO) was introduced to evaluate the quality of the assembly (Grabherr *et al*., 2011). Expression levels of genes were quantified using RNA-Seq by Expectation-Maximization software (RSEM, v1.3.1) (Li & Dewey, 2011). Unigene-encoded protein sequences in unigenes were collected with TransDecoder (v5.5.0) (Kim *et al*., 2015) and calculated against the SwissProt database BLAST. The verified homologous protein sequences and coding regions based on alignments against the Pfam database were predicted using Hmmscan. GO and KEGG databases were used to match unigenes and their possible functions, including transcription factor roles. DESeq2 (v1.4.5) was chosen to separate the DEGs (Wang *et al*., 2010), with the criteria of Q value ≤0.05 or FDR ≤0.001. A heatmap of distinct DEG clusters was produced through the pheatmap function. Functional annotation of DEGs was performed using hypergeometric distribution analysis with the phyper function in R software (https://en.wikipedia.org/wiki/Hypergeometric_distribution) for KEGG enrichment and the TermFinder package (https://metacpan.org/pod/GO::TermFinder) for GO enrichment. Genes with significant enrichment were identified based on a Q value ≤0.05.

Nontargeted metabolic profiling: For nontargeted metabolomic analysis, six biological replicates per group were prepared using standard equipment, including an Eppendorf 5430 low-temperature, a weaving tissue grinder (JXFSTPRP), a QL-901 high-speed centrifuge (Thermo Scientific, USA), a Milli-Q water purification system (Integral Millipore Corporation, USA), and a Maxi Vac Beta refrigerated vacuum concentrator (GENE Company). Reagents included LCMS-grade methanol (A454-4) and acetonitrile (A998-4) from Thermo Fisher Scientific (USA), ammonium formate (17843-250G, Honeywell Fluka, USA), formic acid (FA, 50144-50ml, DIMKA, USA), and internal controls (, 13C3-Progesteron, d5-Tryptophan, d3-Leucine and13C9-Phenylalaninee).

Each 50-µg sample was homogenized in a Eppendorf (1.5-mL) tube with 800 µL of precooled extraction solution (methanol: H2O = 7:3) and 20 µL of internal standard 1 (IS1). The samples were homogenized for 10 min using a tissue grinder set to 50 Hz, followed by ultrasonication, 1-hour incubation without shaking at -20°C, and centrifugation (14,000 rpm at 4°C for 15 min). A 600-µL aliquot of each supernatant was filtered through a 0.22-µm filter, and 20 µL of the filtered supernatants were pooled to generate a quality control (QC) sample for evaluating LC-MS quality.

ACQUITY UPLC I-Class Plus ultra-high-performance liquid chromatography (UPLC) system (Waters, USA) was introduced to display LC-MS experiment, coupled with a Q Exactive high-resolution mass spectrometer (Thermo Scientific). Chromatographic separation of a 5-µL injection volume per sample was completed by a Hypersil GOLD aQ column (100 mm × 2.1 mm, 1.9 µm, Thermo Scientific) with mobile phases of 0.1% FA in water (Phase A) and 0.1% FA in acetonitrile (Phase B) delivered at a flow rate of 0.3 mL/min under the following gradient conditions: 5% Phase B 0.0-2.0 min, 5-95% Phase B 2.0-22.0 min, hold at 95% Phase B 22.0-27.0 min, and washing with 95% Phase B 27.1-30 min. The column temperature was maintained at 40°C.

MS data (necessary and non-necessary) were produced through scan ranges (positive isons, 125-1500 m/z; negative ions, 100-1500 m/z; automatic gain control (AGC) target of 1e6; a resolution of 70,000; maximum ion injection time, 100 ms). The top three precursors were subjected to MS/MS fragmentation with the following conditions: the max-ion injection time, 50 ms; 30,000 resolution; AGC set to 2e5; the stepped normalized collision energy settings, 20, 40, and 60 eV). The ESI parameters were presented as: the auxiliary gas flow rate is 10; the sheath gas flow rate is 40; the negative-ion mode |KV| is 3.20; capillary temperature is 320 °C; the positive-ion mode spray voltage (|KV|) is 3.80; and auxiliary gas heater temperature is 350°C.

Data were processed using Compound Discoverer 3.3 (Thermo Scientific, https://mycompounddiscoverer.com/) and further analyzed with the mzCloud database, BMDB, and the ChemSpider online database, resulting in a data matrix along with the below items, metabolite peak areas and the identified results. The obtained data were thereafter recollected through using Compound Discoverer 3.3 with parameters presented as: parent ion mass deviation < 5 ppm, retention time deviation < 0.2 min mass deviation of fragment ions < 10 ppm. Peak area-based data normalization was performed using probabilistic quotient normalization (PQN) (Guida *et al*., 2016), and batch effects were corrected using QC-based robust locally estimated scatterplot smoothing (LOESS) signal correction (QC-RLSC) (Dunn *et al*., 2011). Metabolites with coefficients of variation exceeding 30% were excluded, and the remaining data underwent log2 transformation. Next, partial least squares-discriminant analysis (PLS-DA) and orthogonal PLS-DA (OPLS-DA), incorporating orthogonal signal correction (OSC) were employed to decompose the X matrix into Y-related and unrelated components. This approach reduced model complexity while enhancing its explanatory capability and predictive power. The data were further analyzed using Pareto scaling and 7-fold cross-validation to construct a robust OPLS-DA model for comparative purposes.

Quantitative real-time (qRT) PCR analysis: We conducted qRT-PCR to validate the expressed levels of selected genes through RNA-Seq. RNA samples from *D. roosii* were converted into cDNA, with three technical replicates produced for qPCR using AceQ® qPCR SYBR Green Master Mix (Low ROX Premixed) and a RT-PCR System (Roche, LightCycler 480 II). We thereafter the single amplicons through melting curve analysis and gel electrophoresis. Cycle threshold (CT) values were normalized to reference genes then relative fold changes were determined according to the ΔΔCT method as previously described (Livak *et al*., 2001).

Results

DEG analysis in *D. roosii* leaves across two developmental stages: To investigate the molecular basis for physiological changes during the growth and development of *D. roosii* leaves, we used an RNA-Seq Analyzer II system to conduct comprehensive transcriptome analysis. This analysis targeted differential gene expression across two leaf developmental stages, utilizing six cDNA libraries derived from total RNA preparations. Each sample yielded over 45.44 million raw reads, resulting in an estimated 44.08 million high-quality reads per sample (Table 1). For the sample, data reliability was confirmed by a high Q30 score of ≥92.79%.

The combined reads with high-quality from both developmental stages provided an extensive overview of the *D. roosii* transcriptome. De novo assembly of these reads, performed using Trinity software, produced 82,476 unigenes, the average length is 1,292 base groups (Fig. 2A). Open reading frames (ORFs) were discovered using TransDecoder, generating a comprehensive dataset of nucleotide and protein sequences suitable for applications such as gene cloning, phylogenetic studies, and functional analysis. Among these unigenes, 19,102 exhibited high-integrity ORFs with complete coding sequences obtained from start to stop codons (Fig. 2B). Distinct yet consistent transcriptomic profiles were observed across biological replicates for the different developmental stages.

Gene expression changes were quantified by evaluating the abundance of gene transcripts, expressed in fragments per kilobase of transcript per million mapped reads (FPKM). Validation of several genes was performed via qRT-PCR analysis. Strong correlations between RNA-Seq and RT-PCR data were observed, confirming the consistency of gene expression patterns between the two methods (Fig. 3). Additionally, a correlation heat map demonstrated high-level agreement among the three biological replicates.

DEG analysis revealed significant alterations in the *D. roosii* transcriptome during leaf development, as reflected by the 4,577 overexpressed and 5,238 lowexpressed genes in total in Stage2 versus Stage1. The above discoveries suggest a complex regulatory mechanism involving gene expression modulation achieved through signal transduction during leaf development. Further bio-informatic analysis tools including GO (Fig. 2C) and KEGG (Fig. 2D) helped to identify the crucial biological processes and the important pathways which involved in the two developmental stages, highlighting terms such as "plant-pathogen interaction", "biosynthesis of secondary metabolites," and "metabolic pathways".

Metabolic differences between two *D. roosii* leaf developmental stages: Analysis of leaf metabolomic data using principal component analysis (PCA) revealed clear separation between Stage1 and Stage2 samples based on PC1 (49.38%) and PC2 (13.36%) (Fig. 4A). We selected 1,297 metabolites in total, which were grouped into thirty items, with the most abundant belonging to "lipids" (82), "flavonoids" (29), "benzene and derivatives" (27), "others" (26), "carbohydrates" (18), "amino acids (AAs), peptides, and analogues" (17), and "terpenoids" (17). KEGG categorization further classified these metabolites into eighteen groups.

To pinpoint significantly changed metabolites (SCMs) between Stage1 and Stage2 leaves, we analyzed six biological replicates. Among the 1,297 metabolites, 382 exhibited significant differences in accumulation between the two stages: 224 metabolites showed increased accumulation, while 158 showed decreased accumulation in Stage2 compared to Stage1 (Fig. 4B, Fig. 4C). KEGG pathway enrichment analysis revealed SCMs were synthesized through pathways associated with "flavonoid biosynthesis", "phenylpropanoid biosynthesis", and "biosynthesis of secondary metabolites" among others (Fig. 4D).

Transcript-metabolite correlation network: In the post-genomic era, systems biology approaches, such as multi-omics integration, have risen to prominence for elucidating biological processes. We applied canonical correlation analysis (CCA) to create a correlation network linking differential metabolites with key indexes of associated omics data, focusing on metabolites with correlation coefficients $|r| > 0.8$. Ranking the top 20 correlations by p-value or Q-value, the resulting network plot offers a comprehensive perspective on the relationships between differential metabolites and associated omics metrics. By annotating these metabolites and differential indices, such as changes in metabolite concentrations or gene expression levels, to KEGG pathways, a complete network diagram was generated, allowing for visual analysis of metabolite expression associations with various biological phenomena. Pathway enrichment analysis identified biological pathways most significantly linked to these processes, with pathway bubble plots illustrating differential metabolite enrichments across correlated omics pathways (Fig. 5).

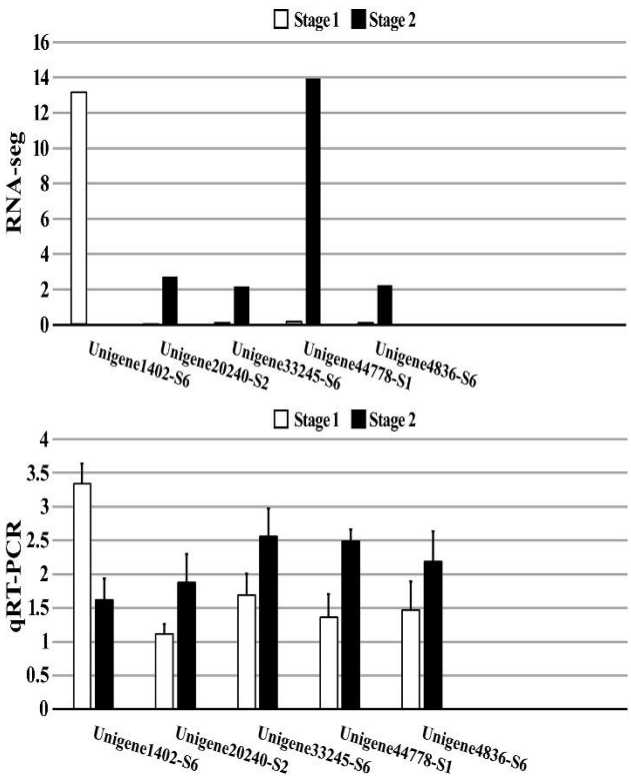

Fig. 3. The qRT-PCR validation of differentially expressed genes of *D. roosii.*

Table 1. Summary of RNA-Seq datasets for the six libraries.

Samples	Total raw reads (M)	Total clean reads (M)	Total clean bases (Gb)	Clean reads Q20 (%)	Clean reads Q30 (%)
Stage 1-1	45.44	44.08	6.61	97.73	93.11
Stage 1-2	46.08	44.29	6.64	97.69	92.92
Stage 1-3	45.76	44.25	6.64	97.65	92.79
Stage 2-1	46.40	44.11	6.62	97.76	93.15
Stage 2-2	45.44	44.11	6.62	97.73	93.10
Stage 2-3	45.44	44.19	6.63	97.66	92.84

-1, -2, and -3: three biological replicates of each leaf sample

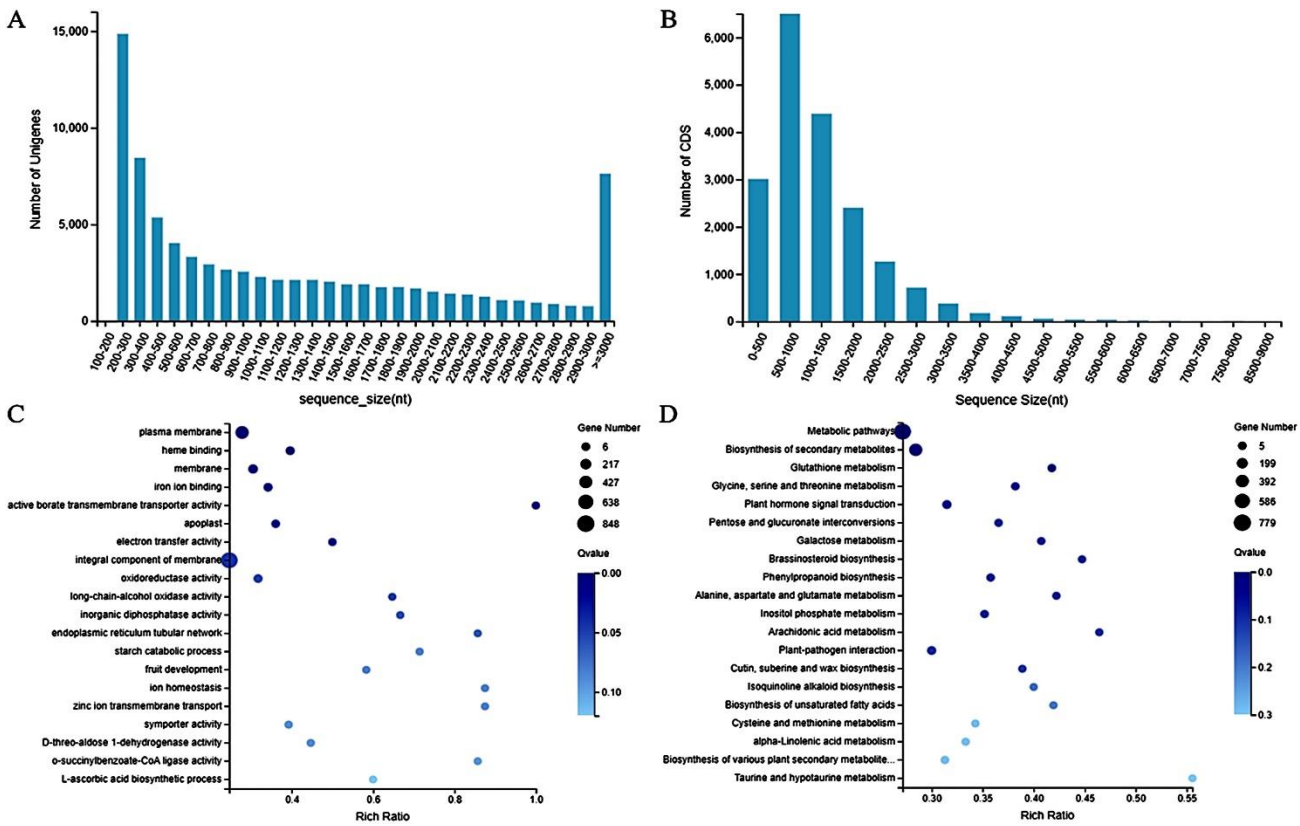

Fig. 2. Genes expressed in two different stages of *D. roosii* leaf development. (A) Assembled transcript length distributions of *D. roosii.* (B) CDS length distributions of *D. roosii.* (C) Analysis of GO terms for differentially expressed genes of *D. roosii* among the two developmental stages. (D) Analysis of KEGG for differentially expressed genes of *D. roosii* among the two developmental stages.

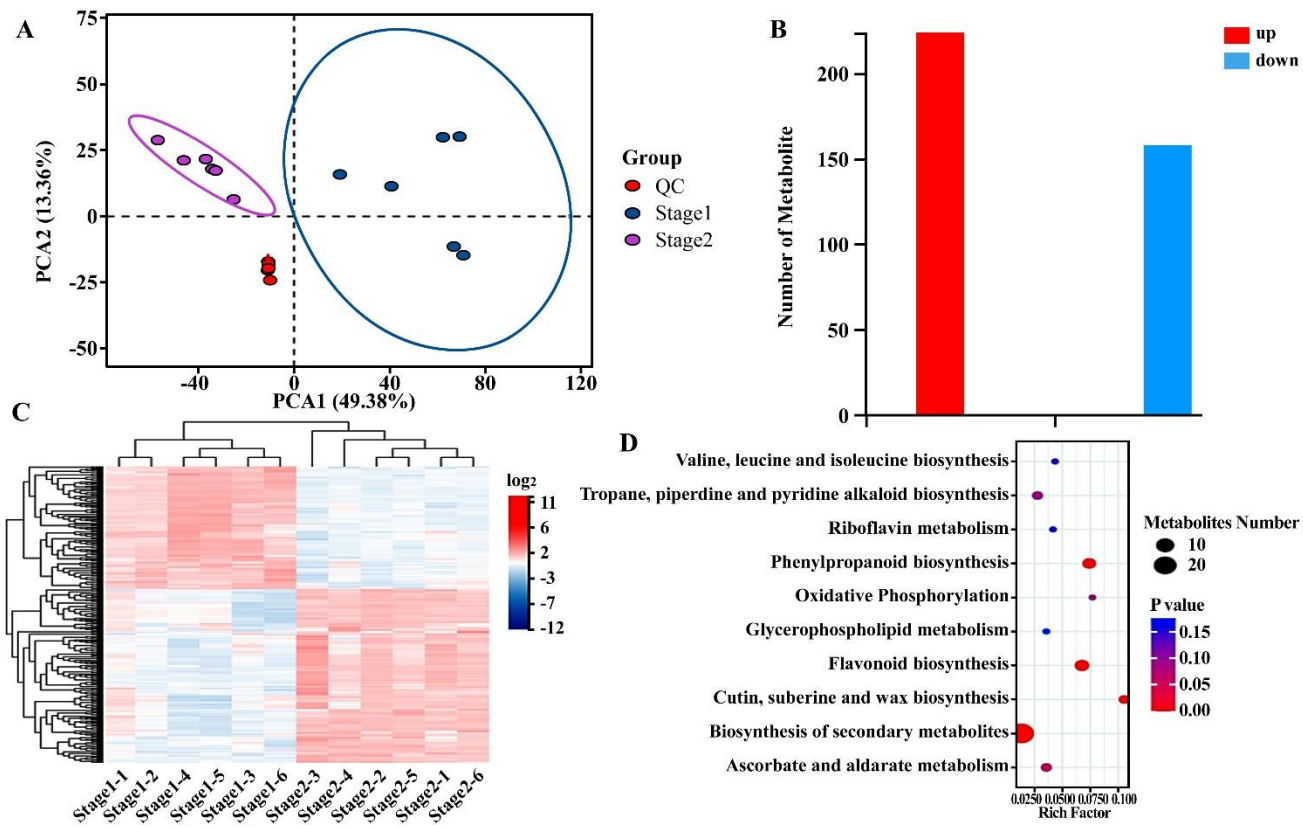

Fig. 4. Characterization of metabolite profiles in *D. roosii* leaves at two developmental stages. (A) Principal Component Analysis (PCA) score plot illustrating the separation of metabolite profiles between Stage 1 and Stage 2 leaves. (B) Number of significantly changed metabolites (SCMs) between Stage 1 and Stage 2 leaves. (C) Heatmap and cluster analysis of metabolite profiles at the metabolome level, comparing different stages of leaf development. (D) KEGG pathway annotation of SCMs identified between the two stages of *D. roosii* leaves.

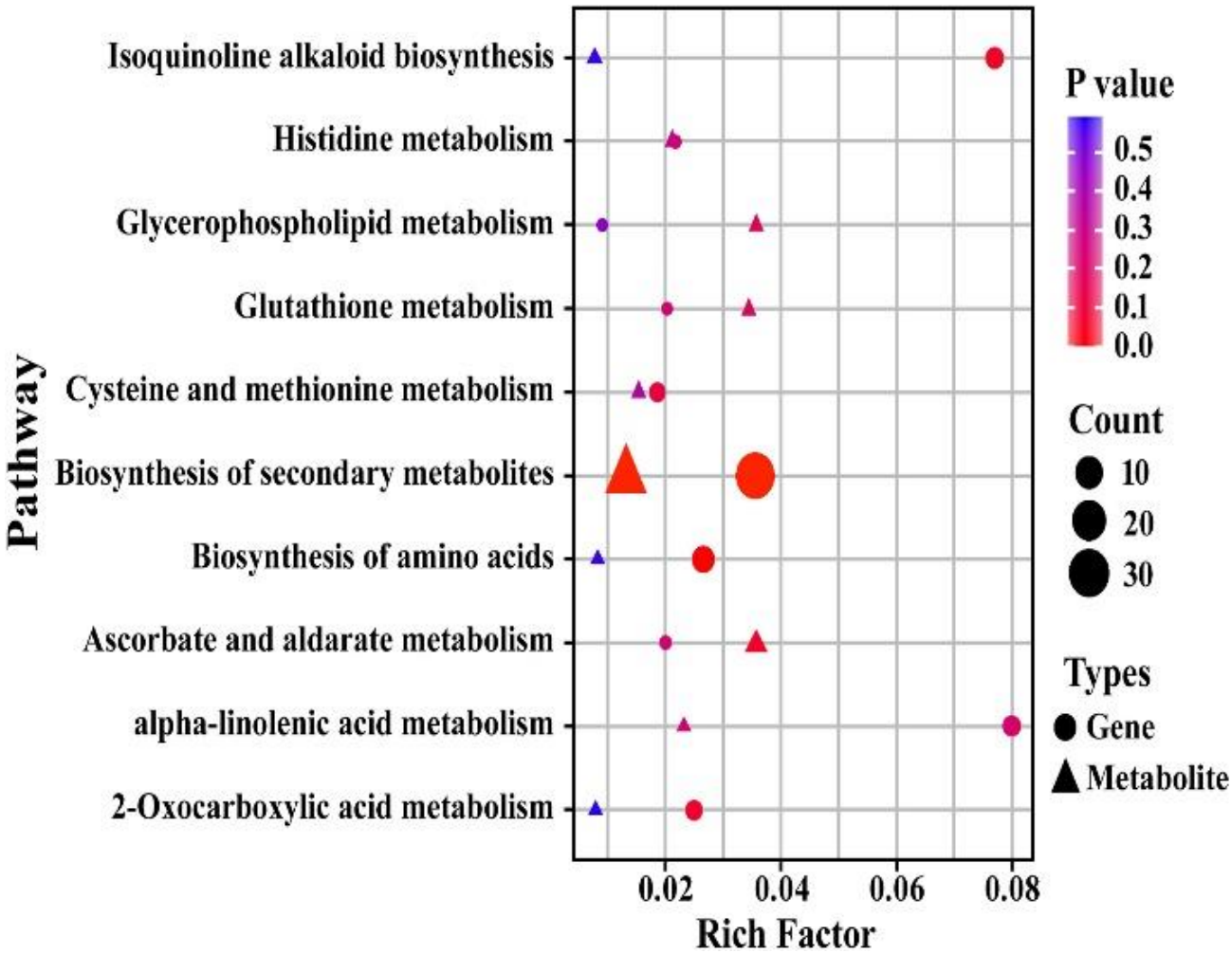

Fig. 5. Pathway enrichment analysis bubble plot. X-axis enrichment factor (richfactor), the larger the value illustrates the greater the proportion of differential metabolites annotated to that pathway and the differential metrics being associated with. The circles represent the indicator pathway of the pathway being associated with omics, the triangles represent metabolic pathways, the graph size represents the number of differential metabolites annotated to that pathway versus the indicator of the difference in the pathway being associated with omics, and the graph color indicates pathway significance.

Discussion

Despite the lack of a published genome for *D. roosii*, a satisfactory annotation rate approaching 33.22% was obtained for unigenes or proteins found in at least one database, which when combined with high correlation coefficients among biological replicates and further validation through qPCR, confirms the high quality of our transcriptome sequence data and our analysis results. The comparative analysis of transcripts between Stage2 and Stage1 samples revealed that *D. roosii* leaf DEGs were predominantly enriched in KEGG pathway terms such as "plant-pathogen interaction", "biosynthesis of secondary metabolites", and "metabolic pathways". Similar pathway enrichments have been observed in studies of *B. campestris* L. (Shi *et al*., 2023), which highlighted leaf developmental pathways including "circadian rhythm", "starch and sucrose metabolism", and "plant hormone signal transduction". Studies on *E. pubescens* (Xu *et al*., 2023) also identified significantly enriched functional terms related to leaf development, such as "RNA transport", "MAPK signaling pathway - plant", and "plant hormone signal transduction".

To expand upon these findings, we investigated the expression levels of TF families with potential roles in regulating these pathways. The strong link between gene expression levels and gene functions suggests crucial roles for TFs in *D. roosii* leaf growth and development. For example, several genes exhibited higher expression in Stage2 compared to Stage1 leaves, including Unigene43668-S5 (PREDICTED: *Ziziphus jujuba* putative 12-oxophytodienoate reductase 11), Unigene44778-S1 (GQ03519_K15 mRNA), Unigene46895-S3 (cellulose synthase catalytic subunit (CesA1) mRNA), Unigene29840-S1 (PREDICTED: *Momordica charantia* TBC1 domain family member 15-like), Unigene42346-S2 (*Trifolium alexandrinum* microsatellite TaSSR267), and Unigene39996-S2 (PREDICTED: *Raphanus sativus* ABC transporter G family member 31). Conversely, genes such as Unigene35404-S3 (isolate PnARF6b auxin response factor 6), Unigene46207-S3 (nuclear/nucleolar GTPase 2), Unigene19646-S5 (DDB1- and CUL4-associated factor homolog 1), Unigene27559-S5 (O-fucosyltransferase 38), Unigene27839-S3 (protein argonaute 1), and Unigene23487-S6 (intron-binding protein aquarius-like) were expressed at lower levels in Stage2 versus Stage1

leaves. These findings highlight TFs with distinct expression patterns during *D. roosii* leaf development and point to TFs specific to different developmental stages, although additional studies are needed to elucidate their roles in these processes.

The extensive differential regulation of genes and metabolites across various metabolic pathways during *D. roosii* leaf development emphasizes the complex nature of this process, which is orchestrated by a complex network encompassing gene interactions and signaling pathways, as exemplified by the detection of 1,297 metabolites spanning thirty substance categories and their derivatives in *D. roosii* leaves during the two developmental stages. This is in contrast to a study by Li *et al*., (2019) utilizing widely targeted metabolite analysis conducted via UPLC-MS in *E. ulmoides*, which identified only 515 metabolites encompassing primarily 127 flavonoids, 16 vitamins, 44 AA derivatives, 46 organic acids, 9 phenolamides, and 8 isoflavones (Li *et al*., 2019), with similar analyses of two rice varieties detecting 512 metabolites in one and 510 in the other (Xue *et al*., 2021).

Our study also identified numerous *D. roosii* leaf SCMs across two developmental stages that likely influence processes impacting leaf morphology, metabolite accumulation, and photosynthetic capacity through their active roles in various metabolic pathways, particularly leaf developmental pathways related to metabolite synthesis and degradation. Notably, significant changes were observed in the levels of metabolites medicarpin 3-O-glucoside-6'-malonate, kaempferol 3-(3"-acetyl-alpha-L-arabinopyranosyl)-(1->6)-glucoside, and flavin mononucleotide, among others. Overall, the accumulation of 382 metabolites in leaves showed significant differences between Stage1 and Stage2, with 224 increasing and 158 decreasing. The discoveries of this research enhance our learning of the complex regulatory networks involved in *D. roosii* leaf development, guiding future research to advance the functional genomics of this important medicinal plant.

Conclusions

This study utilized next-generation sequencing to profile the leaf transcriptome of *D. roosii*, identifying significant differences in gene expression between two distinct developmental stages, with a focus on transcription factors that regulate leaf formation and metabolite production. FPKM analysis unveiled substantial transcriptome changes during leaf development. Additionally, non-targeted metabolomics detected 1,297 compounds across both stages, with lipids representing the most abundant metabolite group.

Acknowledgments

This work was supported by the Guizhou Provincial Basic Research Program (Natural Science) (Grant No. QKHJC-ZK[2024]ZD075); the Guizhou Provincial Foundation for Excellent Scholars Program (Grant No. GCC[2023]077).

References

Chang, N.N., X.P. Yang, X.Q. Wang, C. Chen, C. Wang, Y. Xu, H.Y. Huang and Y. Wang. 2024. Epiphytic patterns impacting metabolite diversity of *Drynaria roosii* rhizomes based on widely targeted metabolomics. *Metabolites*, 14: 409.

Chen, X., X.L. Yang, J. Xie, W.J. Ding, Y.L. Li, Y.Z. Yue and L.G. Wang. 2020. Biochemical and comparative transcriptome analyses reveal key genes involved in major metabolic regulation related to colored leaf formation in *Osmanthus fragrans* 'yinbi shuanghui' during development. *Biomolecules*, 10: 549.

Chen, Y.X., Y.S. Chen, C.M. Shi, Z.B. Huang, Y, Zhang. S.K. Li, Y. Li, J. Ye, C. Yu, Z. Li, X.Q. Zhang, J. Wang, H.M. Yang, L. Fang and Q. Chen. 2018. SOAPnuke: a MapReduce acceleration-supported software for integrated quality control and preprocessing of high-throughput sequencing data. *Gigascience*, 7: 1-6.

Dunn, W.B., D. Broadhurst, P. Begley, E. Zelena, S. Francis-McIntyre, N. Anderson, M. Brown, J.D. Knowles, A. Halsall, J.N. Haselden, A.W. Nicholls, I.D. Wilson, D.B. Kell and R. Goodacre. 2011. Procedures for large-scale metabolic profiling of serum and plasma using gas chromatography and liquid chromatography coupled to mass spectrometry. *Nat. Prot*., 6: 1060-1083.

Gase, K.B.I. 2012. Transformational tools for next-generation plant ecology: Manipulation of gene expression for the functional analysis of genes. *Plant Ecol. Divers.*, 5: 485-490.

Grabherr, M.G., B.J. Haas, M. Yassour, J.Z. Levin, D.A. Thompson, I. Amit, X. Adiconis and L. Fan. 2011. Full-length transcriptome assembly from RNA-seq data without a reference genome. *Nat. Biotech*., 29: 644-652.

Guida, R.D., J. Engel, J.W. Allwood, R.J.M. Weber, M.R. Jones, U. Sommer, M.R. Viant and W.B. Dunn. 2016. Non-targeted UHPLC-MS metabolomic data processing methods: a comparative investigation of normalisation, missing value imputation, transformation and scaling. *Metabolomics*, 12: 93.

Jia, X.L., G.L. Wang, F. Xiong, X.R. Yu, Z.S. Xu, F. Wang and A.S. Xiong. 2015. De novo assembly, transcriptome characterization, lignin accumulation, and anatomic characteristics: novel insights into lignin biosynthesis during celery leaf development. *Sci. Rep*., 5: 8259.

Kim, H.S., B.Y. Lee, E.J. Won, J. Han, D.S.H Wang, H.G. Park and J.S. Lee. 2015. Identification of xenobiotic biodegradation and metabolism-related genes in the copepod *Tigriopus japonicus* whole transcriptome analysis. *Marine Genom*., 3: 207-208.

Lau, W. and E.S. Sattely. 2015. Six enzymes from mayapple that complete the biosynthetic pathway to the etoposide aglycone. *Science*, 349: 1224-1228.

Li, B. and C.N. Dewey. 2011. RSEM: accurate transcript quantification from RNA-Seq data with or without a reference genome. *BMC Bioinform*., 12: 323.

Li, L., M.H. Liu, K. Shi, Z.J. Yu, Y. Zhou, R.S. Fan and Q.Q. Shi. 2019. Dynamic changes in metabolite accumulation and the transcriptome during leaf growth and development in *Eucommia ulmoides*. *Int. J. Mol. Sci*., 20: 4030.

Li, Y., J. Fang, X. Qi, M. Lin, Y. Zhong, L. Sun and W. Cui. 2018. Combined analysis of the fruit metabolome and transcriptome reveals candidate genes involved in flavonoid biosynthesis in *Actinidia arguta*. *Int. J. Mol. Sci*., 19: 1471.

Livak, K.J. and T.D. Schmittgen. 2001. Analysis of relative gene expression data using real-time quantitative PCR and the 2(-Delta Delta C(T)) method. *Methods*, 25: 402-408.

Morozova, O. and M.A. Marra. 2008. Applications of next-generation sequencing technologies in functional genomics. *Genomics*, 92: 255-264.

Nett, R.S., W. Lau and E.S. Sattely. 2020. Discovery and engineering of colchicine alkaloid biosynthesis. *Nature*, 584: 148-153.

Palmer, N.A., R.V. Chowda-Reddy, A.A. Muhle, S. Tatineni, G. Yuen, S.J. Edmé, R.B. Mitchell and G. Sarath. 2019. Transcriptome divergence during leaf development in two contrasting switchgrass (*Panicum virgatum* L.) cultivars. *PLoS One*, 14: e0222080.

Shi, F.Y., Z.F. Zhao, Y. Jiang, S. Liu, C. Tan, C.H. Liu, X.L. Ye and Z.Y. Liu. 2023. Whole transcriptome analysis and construction of a ceRNA regulatory network related to leaf and petiole development in Chinese cabbage (*Brassica campestris* L. ssp. pekinensis). *BMC Genom*., 24: 144.

Shivakumar, V.S., G. Johnson and E.A. Zimmer. 2019. Transcriptome analysis of the curry tree (*Bergera koenigii* L., Rutaceae) during leaf development. *Sci. Rep*., 9: 4230.

Sun, M.Y., J.R. Li, D. Li and L. Shi. 2017. Complete chloroplast genome sequence of the medical fern *Drynaria roosii* and its phylogenetic analysis. Mitochondrial DNA PART B, 2: 7-8.

Sun, M.Y., J.Y. Li, D. Li, F.J. Huang, D. Wang, H. Li, Q. Xing, H.B. Zhu and L. Shi. 2018. Full-length transcriptome sequencing and modular organization analysis of the naringin/neoeriocitrin-related gene expression pattern in *Drynaria roosii*. *Plant Cell Physiol*., 59: 1398-1414.

Töpfer, N., S. Kleessen and Z. Nikoloski. 2015. Integration of metabolomics data into metabolic networks. *Front. Plant Sci*., 6: 49.

Wang, L.K., Z.X. Feng, X. Wang, X.W. Wang and X.G. Zhang. 2010. DEGseq: an R package for identifying differentially expressed genes from RNA-seq data. *Bioinformatics*, 26: 136-138.

Wufuer, H., Y.C. Xu, D. Wu, W.W. He, D.Y. Wang, W.M. Zhu and L.P. Wang. 2022. Liglaurates A-E, cytotoxic bis (lauric acid-12yl) lignanoates from the rhizomes of *Drynaria roosii* Nakaike. *Phytochemistry*, 198: 113143.

Xu, C.Q., X. Liu, G.A. Shen, X.L. Fan, Y. Zhang, C. Sun, F.M. Suo and B.L. Guo. 2023. Time-series transcriptome provides insights into the gene regulation network involved in the icariin-flavonoid metabolism during the leaf development of *Epimedium pubescens*. *Front. Plant Sci.*, 14: 1183481.

Xue, J., D.B. Lu, S.G. Wang, Z.H. Lu, W. Liu, X.F. Wang, Z.Q. Fang and X.Y. He. 2021. Integrated transcriptomic and metabolomic analysis provides insight into the regulation of leaf senescence in rice. *Sci. Rep*., 11: 14083.

Zhang, X., X.L. Ding, Y.X. Ji, S.C. Wang, Y.Y. Chen, J. Luo, Y.B. Shen and L. Peng. 2018. Measurement of metabolite variations and analysis of related gene expression in Chinese liquorice (*Glycyrrhiza uralensis*) plants under UV-B irradiation. *Sci. Rep*., 8: 6144.

Zhu, G.T., S.C. Wang, Z.J. Huang, S.B. Zhang, Q.G. Liao, C.Z. Zhang, T. Lin, M. Qin, M. Peng, C.K. Yang, X. Cao, X. Han, X.X. Wang, E. Knaap, Z.H. Zhang, X. Cui, H. Klee, A.R. Fernie, J. Luo and S.W. Huang. 2018. Rewiring of the fruit metabolome in tomato breeding. *Cell*, 172: 249-261.

(Received for publication 2 October 2024)